

A lattice Boltzmann equation method for real fluids with the equation of state known in tabular form only in regions of liquid and vapor phases[☆]

Alexander L. Kupershtokh^{*}

Lavrentyev Institute of Hydrodynamics of Siberian Branch of Russian Academy of Sciences, Lavrentyev prosp. 15, Novosibirsk, 630090, Russia

ARTICLE INFO

Article history:

Received 11 October 2009

Received in revised form 17 June 2010

Accepted 18 June 2010

Keywords:

Lattice Boltzmann equation

Equation of state

Phase transition

Two-phase flows

Surface tension

ABSTRACT

We propose several simple interpolations of the isotherms for real fluids in the region below the binodal curve, where data concerning the equation of state is absent, especially in the thermodynamically prohibited region. All interpolations satisfy the boundary conditions at the points on the binodal curve. The Maxwell rule is also fulfilled. As an example, we construct several isotherms for real water. The data for the isotherms of water, in the liquid and vapor states, is given in tabular form. All smooth interpolations of the isotherms show similar hydrodynamic behavior of two-phase systems in LBE simulations. The reduced specific volumes of the liquid and vapor phases and the reduced pressure on the binodal curve obtained in the LBE simulations for the different interpolations agree well with the experimental data for real EOS of water. The surface tension depends on the form of the interpolation of the isotherm under the binodal curve. Hence, the value of surface tension can be varied in some range by changing the interpolation curve. Actually, our variant of the LBE method allows one to obtain the values of the liquid and vapor densities at the interface corresponding to the saturation curve of real fluids with high accuracy. At low temperatures, the large values of the liquid-to-vapor density ratio can be obtained, in accordance with the EOS of real fluids.

© 2010 Elsevier Ltd. All rights reserved.

1. Introduction

In LBE methods, the different phases of a substance are usually simulated as one fluid. As a result, there is no need to track the interfaces between the vapor and liquid phases. These interfaces are represented as thin transition layers (Fig. 1) of finite width (several lattice nodes). These interfaces can appear, disappear and undergo topological changes.

The LBE method of simulation of multiple phases was first proposed by Shan and Chen in [1]. This original method involves explicit pair interaction between every pair of neighboring nodes. A second approach is based on the free energy [2]. This latter approach ensures that the interface layers have a constant width. Unfortunately, the temperature dependence of the surface tension is incorrect in this approach. Qian and Chen [3] proposed a way to include the real-gas equation of state, given in the analytical form, in the LBE method. For the first time, they introduced the pseudo-potential for the van der Waals equation of state into the Shan and Chen method. Instead of the consideration of pair interactions, the total force acting on the fluid at a node was introduced in the method proposed by Zhang and Chen [4].

After some improvements of this last method, it became possible to describe successfully the binodal (saturation) curve with high accuracy (about 1%) for equations of state (EOS) given in analytical form [5–7]. Hence, the lattice Boltzmann

[☆] This work was supported in part by the Russian Foundation for Basic Research (grant No. 10-08-00805), by the Presidium of RAS (grant No. 12.12-2009) and by the Siberian Branch of the Russian Academy of Sciences (grants No. 58-2009 and No. 116-2009).

^{*} Tel.: +7 383 3361163; fax: +7 383 3333332.

E-mail address: skn@hydro.nsc.ru.

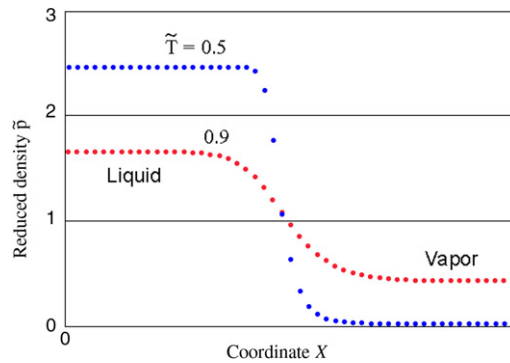


Fig. 1. Liquid–vapor transition layers at different reduced temperatures \tilde{T} . Both curves correspond to the van der Waals EOS.

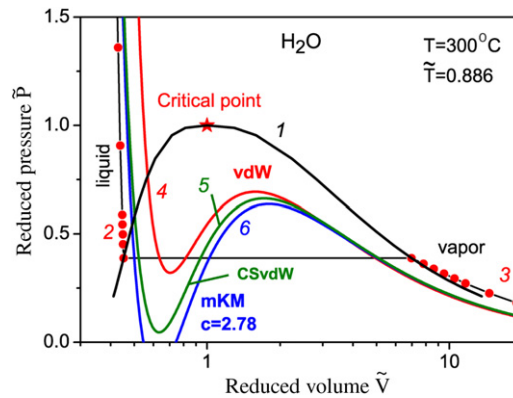


Fig. 2. Binodal curve (curve 1), the liquid (curve 2) and the vapor (curve 3) wings of the isotherm at 300 °C for the real EOS of water [8]. Isotherms for the van der Waals EOS (curve 4), the Carnahan–Starling–van der Waals EOS (curve 5), and the modified Kaplun–Meshalkin EOS [7] (curve 6).

equation (LBE) method can be used for simulating fluid flows with interfaces between the vapor and liquid phases. However, the analytical equations of state – such as the van der Waals EOS (vdW), the Carnahan–Starling–van der Waals EOS (CSvdW), and the modified Kaplun–Meshalkin EOS (mKM) – describe the isotherm of real fluids very inaccurately (Fig. 2).

For the purpose of simulating the transition between phases, the special forces between neighboring nodes should be included in the LBE algorithm. One convenient implementation is the method proposed by Zhang and Chen [4]. They considered the total force \mathbf{F} acting on a node. This force was represented by the gradient of the special pseudo-potential U :

$$\mathbf{F} = -\nabla U, \tag{1}$$

$$U = P(\rho, T) - \rho\theta, \tag{2}$$

where $P(\rho, T)$ is the desired equation of state, θ is the “kinetic temperature” of pseudo-particles in LBE models, and T is the physical temperature of the fluid. These forces implicitly determine the vapor–liquid coexistence curve and ensure the surface tension at the interface. For specific fluids, the real EOS can be constructed from the tabular experimental data on the isotherms in the regions corresponding to the liquid and vapor phases. On the other hand, the experimental data below the binodal curve in the pressure–volume diagram is very restricted, only being available for metastable regions. The experimental data on the states below the spinodal curve (in the thermodynamically prohibited region) cannot be obtained at all. However, this part of the isotherm should be defined, because the LBE method considers the interfaces between the vapor and liquid phases as transition layers, in which the states of the fluid change continuously from the liquid to the vapor phase along the isotherm (Fig. 1).

2. Lattice Boltzmann equation method

We use the usual evolution equation [9,10]

$$N_k(\mathbf{x} + \mathbf{c}_k \Delta t, t + \Delta t) = N_k(\mathbf{x}, t) + \Omega_k + \Delta N_k, \tag{3}$$

where \mathbf{c}_k are the velocity vectors of LBE pseudo-particles, Δt is the time step, Ω_k is the collision operator, and ΔN_k is the change in the distribution function due to the action of the body force.

The discrete set of the velocity vectors \mathbf{c}_k depends on the lattice geometry. In the present work, we use the standard one-dimensional LBE model D1Q3 with three velocity vectors $|\mathbf{c}_k| \in \{0, h/\Delta t\}$ and the standard two-dimensional LBE model D2Q9 with nine velocity vectors $|\mathbf{c}_k| \in \{0, h/\Delta t, \sqrt{2}h/\Delta t\}$ on a square lattice [11]. Here, h is the lattice spacing.

The fluid density ρ and the velocity \mathbf{u} at a node are calculated as

$$\rho = \sum_k N_k, \quad \rho \mathbf{u} = \sum_k \mathbf{c}_k N_k. \tag{4}$$

We use two types of collision operator. The first type is the SRT (single relaxation time) collision operator (also known as the BGK collision operator)

$$\Omega_k = \frac{N_k^{\text{eq}}(\rho(\mathbf{x}, t), \mathbf{u}(\mathbf{x}, t)) - N_k(\mathbf{x}, t)}{\tau}. \tag{5}$$

Here, we use the equilibrium distribution functions $N_k^{\text{eq}}(\rho, \mathbf{u})$ in the standard form

$$N_k^{\text{eq}}(\rho, \mathbf{u}) = \rho w_k \left(1 + \frac{\mathbf{c}_k \mathbf{u}}{\theta} + \frac{(\mathbf{c}_k \mathbf{u})^2}{2\theta^2} - \frac{\mathbf{u}^2}{2\theta} \right). \tag{6}$$

For the standard “isothermal” LBE models D1Q3, D2Q9, and D3Q19 [11] with the equilibrium distribution (6), the “kinetic temperature” is equal to $\theta = (h/\Delta t)^2/3$.

The second type of the collision operator which we use is the MRT (multi-relaxation time) collision operator [12,13].

For the implementation of the body force term, we use the method of exact difference [14–17]

$$\Delta N_k(\mathbf{x}, t) = N_k^{\text{eq}}(\rho, \mathbf{u} + \Delta \mathbf{u}) - N_k^{\text{eq}}(\rho, \mathbf{u}), \tag{7}$$

where the change of the velocity

$$\Delta \mathbf{u} = \mathbf{F} \Delta t / \rho \tag{8}$$

is defined by the force \mathbf{F} acting on the node. This implementation of the body force term is very simple and it is superior to other implementations (see [5–7]). It can be used for any form of the collision operator, including both SRT and MRT.

It is convenient to use the reduced variables $\tilde{P} = P/P_{cr}$, $\tilde{\rho} = \rho/\rho_{cr}$, and $\tilde{T} = T/T_{cr}$ in the LBE algorithm, where P_{cr} , ρ_{cr} , and T_{cr} are the values of pressure, density and temperature at the critical point. We use the reduced variables not only for the EOS, but also for the LBE distribution functions $\tilde{N}_k = N_k/\rho_{cr}$, velocity $\tilde{\mathbf{u}} = \mathbf{u}\Delta t/h$, “kinetic temperature” $\tilde{\theta} = \theta(\Delta t/h)^2$, and potential $\tilde{U} = U(\Delta t/h)^2/\rho_{cr}$. Therefore, we obtain from (2) the expression for the reduced pseudo-potential:

$$\tilde{U} = k\tilde{P}(\tilde{\rho}, \tilde{T}) - \tilde{\rho}\tilde{\theta}. \tag{9}$$

The dimensionless coefficient

$$k = \frac{P_{cr}}{\rho_{cr}} \left(\frac{\Delta t}{h} \right)^2 \tag{10}$$

plays an important role in the numerical stability of LBE simulations [7,17].

In order to simulate precisely the binodal curve and transition layers, we proposed to use the following in the LBE method:

- the isotropic finite difference approximation of the potential gradient (1) on a lattice [6,7],
- the method of exact difference mentioned above, and
- a relatively small $\Delta t/h$ ratio (the hydrodynamic Courant number $\tilde{c} = c_s \Delta t/h$ should be less than the critical number $\tilde{c}_{cr} = \sqrt{1 + \tilde{\theta}}$ [17]), required for the numerical stability of the LBE algorithm with a given equation of state of a fluid [7, 17].

Earlier, we proposed the isotropic finite difference approximation of the gradient of the potential \tilde{U} on a lattice [6,7], using a single free parameter A

$$\mathbf{F}(\mathbf{x}) = \frac{1}{\alpha h} \left[A \sum_k \frac{G_k}{G_0} \Phi^2(\mathbf{x} + \mathbf{e}_k) \mathbf{e}_k + (1 - 2A) \Phi(\mathbf{x}) \sum_k \frac{G_k}{G_0} \Phi(\mathbf{x} + \mathbf{e}_k) \mathbf{e}_k \right], \tag{11}$$

where $\mathbf{e}_k = \mathbf{c}_k \Delta t$ are the vectors to the neighboring nodes and $\Phi^2 = -U$. The coefficient α is equal to 1, 3/2, and 3 for the one-dimensional model D1Q3, the two-dimensional model D2Q9, and the three-dimensional model D3Q19, respectively. Here, G_k are coefficients which differ for the basic and diagonal directions of the lattice. The coefficients G_k for diagonal directions, which ensure the isotropy of space, are equal to 0, $G_0/4$, and $G_0/2$ for the models D1Q3, D2Q9, and D3Q19, respectively.

Below, we will omit the sign “~” for all reduced variables.

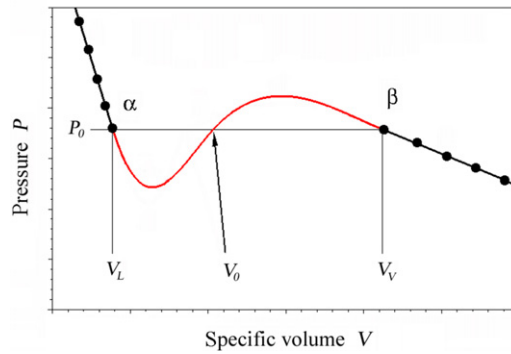


Fig. 3. Typical isotherm on the P - V diagram.

3. Interpolation of isotherms

To define the isotherm curve under the binodal curve, it is necessary to extrapolate smoothly the experimental data to the metastable regions of the fluid states and to construct the isotherm in the “prohibited” region in accordance with the Maxwell rule.

The different interpolations of the isotherm below the binodal curve can influence the value of the surface tension, but should determine the definite values of the pressure and the specific volumes of the liquid and vapor phases. Obviously, every form of the interpolating function should be rather smooth. Moreover, the interpolations should be reasonable. Extraneous oscillations of an interpolating function under the binodal curve should be absent.

The surface tension at the interface, between the liquid and vapor phases, is related to the excess of the Gibbs free energy in the interface layer. Along the isotherm, the Gibbs free energy has the form

$$G = PV - \int P dV + \varphi(T), \tag{12}$$

where $\varphi(T)$ is an arbitrary function of a temperature [18]. The value of the surface tension can be varied in some range by changing the form of the interpolation curve $P = f(V)$.

In the present work, we propose several interpolations of the isotherm in the region below the binodal curve $V_l < V < V_v$. Here, V_l and V_v are the equilibrium values of specific volume for the liquid and vapor phases, respectively, near the flat interface at the given temperature. The pressure on the isotherm at the points $V = V_l$ and $V = V_v$ (Fig. 3) on the binodal curve is defined by the equation of state and is equal to

$$P_0 = P(T, V_l) = P(T, V_v). \tag{13}$$

The slopes of the isotherm at these points are equal to

$$\alpha = \left(\frac{\partial P(T, V)}{\partial V} \right)_{V=V_l}, \quad \beta = \left(\frac{\partial P(T, V)}{\partial V} \right)_{V=V_v}. \tag{14}$$

The values of α and β are negative (Fig. 3).

Every interpolation of an isotherm should satisfy the continuity and smoothness conditions at the points on the binodal curve

$$f(V_l) = P_0, \quad f(V_v) = P_0, \tag{15}$$

$$\left(\frac{df}{dV} \right)_{V=V_l} = \alpha, \quad \left(\frac{df}{dV} \right)_{V=V_v} = \beta. \tag{16}$$

Moreover, the Maxwell rule should be also satisfied

$$\int_{V_l}^{V_v} (f(V) - P_0) dV = 0. \tag{17}$$

Eq. (17) reflects the fact that the Gibbs free energy (12) has equal values at liquid and vapor phases that are in equilibrium.

The first piecewise interpolation consists of two half-periods of different sinusoidal curves, shifted upward by the pressure P_0 (Fig. 4, curve 3). The corresponding solution is derived in analytical form

$$\begin{aligned} f_1(V) &= P_0 - A \sin \left(\pi \frac{V - V_l}{V_0 - V_l} \right) \quad \text{at } V_l < V < V_0, \\ f_2(V) &= P_0 + B \sin \left(\pi \frac{V - V_0}{V_v - V_0} \right) \quad \text{at } V_0 < V < V_v. \end{aligned} \tag{18}$$

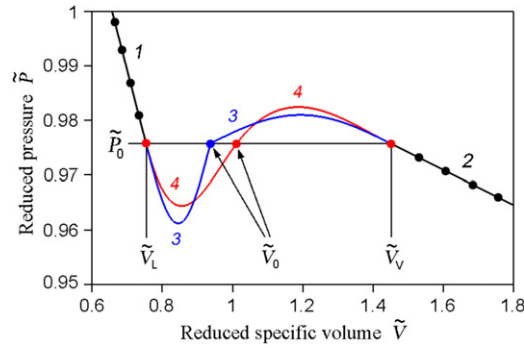


Fig. 4. Isotherm on the P - V diagram. Curves 1 and 2 are the liquid and vapor wings of the water isotherm at $371.9\text{ }^\circ\text{C}$ obtained from the tabular form of the EOS of water [8]. Curves 3 and 4 are the piecewise interpolations of the isotherm in the sinusoidal form (18) and in the spline form (26), respectively, in the region under the binodal curve.

In this case, the continuity condition

$$f_1(V_0) = f_2(V_0) = P_0 \tag{19}$$

is also satisfied at the point $V = V_0$.

The parameters V_0 , A , and B can be found analytically from (16) and (17)

$$V_0 = V_l + (V_v - V_l) \frac{\sqrt{\alpha\beta} + \beta}{\beta - \alpha}, \tag{20}$$

$$A = -\frac{\alpha(V_0 - V_l)}{\pi}, \quad B = -\frac{\beta(V_v - V_0)}{\pi}. \tag{21}$$

From (18), we obtain the Maxwell rule in the form

$$B = A \frac{V_0 - V_l}{V_v - V_0}. \tag{22}$$

Obviously, if $\beta = \alpha$, then the following equations should be used

$$V_0 = \frac{V_v + V_l}{2}, \quad A = B = -\frac{\alpha}{\pi} \frac{(V_v - V_l)}{2}. \tag{23}$$

Note that this interpolation of the isotherm is not smooth at the point $V = V_0$.

The second possible interpolation of $f(V)$ is a piecewise polynomial approximation that also consists of two segments. In this paper, we use the quadratic polynomials

$$\begin{aligned} f_1(V) &= b_1V^2 + c_1V + d_1 \quad \text{at } V_l < V < V_0, \\ f_2(V) &= b_2V^2 + c_2V + d_2 \quad \text{at } V_0 < V < V_v. \end{aligned} \tag{24}$$

Seven unknown parameters $b_1, c_1, d_1, b_2, c_2, d_2$, and V_0 can be found as the numerical solution of the system of seven Eqs. (15)–(17) and (19). The additional conditions $b_1 > 0$ and $b_2 < 0$ are used to choose from the possible solutions. Unfortunately, this form of the interpolation is also not smooth at the intermediate point $V = V_0$. However, the seven unknown parameters of approximation can be found analytically in this case. The position of intermediate point V_0 is defined again by the formula (20). The final solution has the form

$$\begin{aligned} f_1(V) &= P_0 - \frac{\alpha}{V_0 - V_l} (V - V_0)(V - V_l), \quad \text{at } V_l < V < V_0, \\ f_2(V) &= P_0 + \frac{\beta}{V_v - V_0} (V - V_0)(V - V_v), \quad \text{at } V_0 < V < V_v. \end{aligned} \tag{25}$$

The third possible interpolation of $f(V)$ is a spline function $s(V)$, which also consists of two segments

$$\begin{aligned} s_1(V) &= a_1V^3 + b_1V^2 + c_1V + d_1 \quad \text{at } V_l < V < V_0, \\ s_2(V) &= a_2V^3 + b_2V^2 + c_2V + d_2 \quad \text{at } V_0 < V < V_v. \end{aligned} \tag{26}$$

The additional conditions at the intermediate point $V = V_0$ are

$$s_1(V_0) = P_*, \quad s_2(V_0) = P_*, \tag{27}$$

$$\left(\frac{ds_1}{dV}\right)_{V=V_0} = \left(\frac{ds_2}{dV}\right)_{V=V_0}. \tag{28}$$

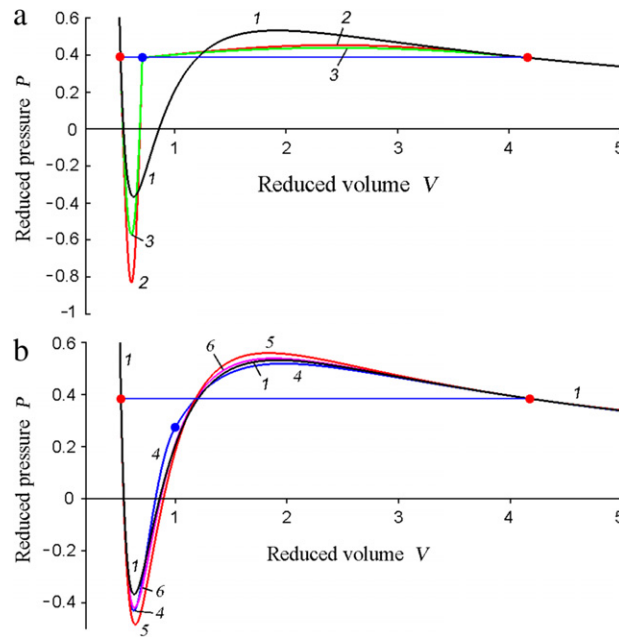


Fig. 5. The different interpolations of the isotherm at $\tilde{T} = 0.8$. Curve 1 are the original isotherm for the van der Waals EOS. Curve 2 is the sinusoidal interpolation (18). Curve 3 is the polynomial interpolation (25). Curve 4 is the spline interpolation (29) at $V_0 = 1$ and $P_* = 0.27$. Curves 5 and 6 are the interpolations (30) with the sets of power exponents (31) and (32), respectively.

The possible position of the intermediate point V_0 and the pressure P_* at this point are the free parameters that can be varied within certain ranges.

Eight unknown parameters $a_1, b_1, c_1, d_1, a_2, b_2, c_2, d_2$ of the spline function $s(V)$ are the solution of the system of eight Eqs. (15)–(17), (27)–(28). Unfortunately, these eight parameters can be found only numerically. This interpolation of the isotherm for water, at the temperature 371.9 °C, by the spline function (26) is shown in Fig. 4 (curve 4). However, numerical tests show that the interpolation by the spline function in the form (26), as the function of the specific volume, can be used only in the region close to the critical point.

Better results for lower temperatures can be obtained using a spline function of the form

$$\begin{aligned} s_1(V) &= a_1\rho^3 + b_1\rho^2 + c_1\rho + d_1 \quad \text{at } V_l < V < V_0, \\ s_2(V) &= a_2\rho^3 + b_2\rho^2 + c_2\rho + d_2 \quad \text{at } V_0 < V < V_v. \end{aligned} \tag{29}$$

Here, $\rho = 1/V$ is the density. The same conditions should be used also in this case (15)–(17), (27)–(28). The possible position of the intermediate point V_0 and the pressure P_* are the free parameters, as for the previous interpolation. Hence, eight unknown coefficients of the spline function (29) are the solution of these eight equations, as in the previous case.

The next possible interpolation of $f(V)$ is the polynomial interpolation with respect to the density ρ , in the form

$$f(V) = a\rho^{n_1} + b\rho^{n_2} + c\rho^{n_3} + d\rho^{n_4} + h\rho^{n_5}. \tag{30}$$

Here, n_i are the arbitrary integer power exponents. The simplest particular sets of the power exponents are

$$n_1 = 4, \quad n_2 = 3, \quad n_3 = 2, \quad n_4 = 1, \quad n_5 = 0, \tag{31}$$

and

$$n_1 = 5, \quad n_2 = 4, \quad n_3 = 3, \quad n_4 = 2, \quad n_5 = 1. \tag{32}$$

Five undefined coefficients a, b, c, d, h can be found from the solution of the system of five Eqs. (15)–(17).

4. Tests for the van der Waals equation of state

To compare the different interpolations, we used the van der Waals equation of state in reduced variables

$$\tilde{P} = \frac{8\tilde{\rho}\tilde{T}}{3 - \tilde{\rho}} - 3\tilde{\rho}^2 \tag{33}$$

for which the isotherm under the binodal curve is well defined.

The different interpolations of the isotherm under the binodal curve for the vdW EOS are shown in Fig. 5.

Table 1
Reduced specific volume and reduced pressure on the binodal curve for the vdW EOS.

\tilde{T}	Lattice Boltzmann simulations						Theory
	Eq. (18)	Eq. (25)	Eq. (29)	Eq. (30), set (31)	Eq. (30), set (32)	vdW	
Reduced specific volume of the liquid state							
0.8	0.51752	0.51756	0.51739	0.51738	0.51739	0.51739	0.517409
0.6	0.432604	0.43262	0.43262	0.43259	0.432604	0.432608	0.432609
Reduced specific volume of the vapor state							
0.8	4.209	4.220	4.167	4.163	4.166	4.1665	4.1725
0.6	16.627	16.940	16.911	16.384	16.625	16.696	16.729
Reduced pressure							
0.8	0.38112	0.38041	0.38370	0.38392	0.38376	0.38373	0.38336
0.6	0.08728	0.08584	0.08594	0.08842	0.8733	0.8702	0.08687

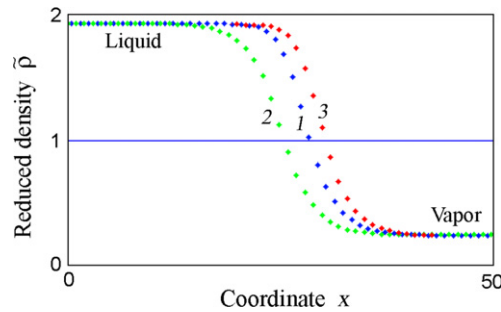


Fig. 6. Liquid–vapor transition layers. Curve 1 is obtained for the original van der Waals equation of state. Curve 2 is the layer for the piecewise interpolation in the sinusoidal form (18). Curve 3 is the layer for the interpolation in the form (30) with the set of power exponents (32). $\tilde{T} = 0.6$.

Table 2
Number of nodes in the interface layer in LBE simulations.

\tilde{T}	Number of nodes					
	vdW	Nonsmooth interp.		Smooth interpolations		
		Eq. (18)	Eq. (25)	Eq. (29)	Eq. (30), set (31)	Eq. (30), set (32)
0.8	17	18	19	17	16	17
0.6	11	17	18	11	11	11

The coexistence of the vapor and liquid phases in the case of a flat interface between them is studied in the LBE simulations, at different temperatures, for the van der Waals equation of state. The parameters $k = 0.01$ and $A = -0.152$ are used in the simulations. The results (particularly, the reduced specific volumes of the liquid and vapor phases and the reduced pressure on the binodal curve) obtained in the LBE simulations for all interpolations listed above are given in Table 1. Here, the theoretical values for the van der Waals EOS are also shown. As pointed out earlier in [7], there is excellent agreement for the liquid branch of the binodal curve. It should be noted that the results obtained in the LBE simulations using the interpolation (30) with the set of the power exponents (32) are in better agreement with the data on the vapor branch of the binodal curve than the results obtained using other interpolations.

The structures of the flat interfaces in LBE simulations for the vdW EOS (curve 1), for the sinusoidal interpolation (18) (curve 2), and for the interpolation (30) with the set of power exponents (32) (curve 3) are shown in Fig. 6. The width of a transition layer is defined as the region where the density of a fluid is in the range $0.01\Delta\rho < (\rho - \rho_v) < 0.99\Delta\rho$. Here, $\Delta\rho = \rho_l - \rho_v$ is the difference of the liquid and vapor densities. The width of the transition layer is larger for nonsmooth interpolations (sinusoidal (18) and polynomial (25)). Indeed, for $\tilde{T} = 0.6$, the number of nodes in the transition layer is equal to 17 for the sinusoidal interpolation (18), instead of 11 for the vdW EOS (see Table 2).

The reduced values of the surface tension were calculated as a product of the pressure difference and the radius for a round liquid droplet in a saturated vapor, in accordance with the Laplace’s law $\tilde{\sigma} = (\tilde{P}_l - \tilde{P}_v)\tilde{R}$, where \tilde{R} is the reduced droplet radius. The results obtained using different interpolations are shown in Fig. 7 for the three different radii of the droplets. The averaged values of the surface tension for different interpolations of the isotherm are given in Table 3.

The LBE tests of droplet oscillations are carried out both for the original van der Waals equation of state and for the interpolation (30) with the set of power exponents (32). The results are shown in Fig. 8(a) and (b), respectively. The parameters of the simulations are $k = 0.01$, $A = -0.152$, $\tau = 0.6$, $a/b = 1.5$. The period of droplet oscillations \tilde{t}_{LBE}

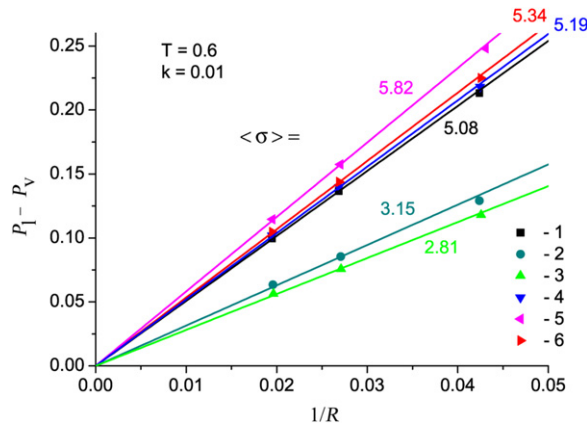


Fig. 7. Laplace law tests for 2D droplets. $\tilde{T} = 0.6$. Curve 1 is the test with the vdW EOS. Curves 2, 3, 4, 5, 6 are the tests with the piecewise sinusoidal interpolation (18), the piecewise parabolic interpolation (25), the spline interpolation (29), the polynomial interpolation (30) with the sets (31) and (32), respectively.

Table 3
Surface tension measured in LBE simulations for different interpolations of the van der Waals EOS.

\tilde{T}	Average surface tension $\langle \sigma \rangle$					
	vdW	Nonsmooth interp.		Smooth interpolations		
		Eq. (18)	Eq. (25)	Eq. (29)	Eq. (30), set (31)	Eq. (30), set (32)
0.8	1.81	1.60	1.44	1.80	1.93	1.85
0.6	5.08	3.15	2.81	5.19	5.82	5.34

Table 4
Droplet oscillations in LBE simulations.

EOS	Interpolation	\tilde{T}	\tilde{t}_{LBE}	$\tilde{\rho}_L$	$\tilde{\sigma}$	$2\tilde{R}$	k	τ	Re	$\tilde{t}_{LBE}/\tilde{t}_0$
vdW	None	0.6	4854	2.319	5.08	88.85	0.01	0.6	42	1.092
vdW	(30) + (32)	0.6	4744	2.319	5.34	88.78	0.01	0.6	43	1.096
H ₂ O	(30) + (31)	0.453	3564	3.12	26.88	85.72	0.005	0.8	19	1.187

for the second case is 1.024 times less than the period for vdW equation of state (see Table 4). This is mainly because of the higher surface tension in the second case.

The theoretical frequency of small oscillations of a spherical liquid droplet for an ideal (non-viscous) fluid has the form [19]

$$\omega^2 = 8\sigma / (\rho R^3). \tag{34}$$

The period of oscillations in reduced variables has the form

$$\tilde{t}_0 = \pi \sqrt{\frac{\tilde{\rho} \tilde{R}^3}{2\tilde{\sigma} k}}, \tag{35}$$

where k is the parameter (10). The values of the ratio of the periods obtained in LBE simulations to the theoretical predictions $\tilde{t}_{LBE}/\tilde{t}_0$ are shown in Table 4. The Reynolds number $Re = \sqrt{d\rho\sigma}/\mu$ is also given in Table 4, where d is the diameter of a droplet and μ is the dynamic viscosity of a liquid. The Reynolds number can be expressed in reduced variables, $Re = \frac{3}{\tau-0.5} \sqrt{2\tilde{R}k\tilde{\sigma}/\tilde{\rho}}$.

Obviously, the period of oscillations for a viscous fluid is somewhat larger than for an ideal fluid. Thus, the results of the dynamic simulations agree well with the theoretical predictions.

However, for nonsmooth interpolations (18) and (25), the droplet oscillations have a nonphysical character (Fig. 8(c)). This is possibly due to different acoustic impedances in the interface layer in the vicinity of the surface $V = V_0$.

5. Tests and simulations for the EOS of water

The comparison of the sinusoidal interpolation (18) and the piecewise polynomial interpolation (25) for the isotherm of water at 100 °C is shown in Fig. 9. The saturation pressure is equal to $P_0 = 0.1014$ MPa. It should be noted that, in both cases, the Maxwell rules are satisfied.

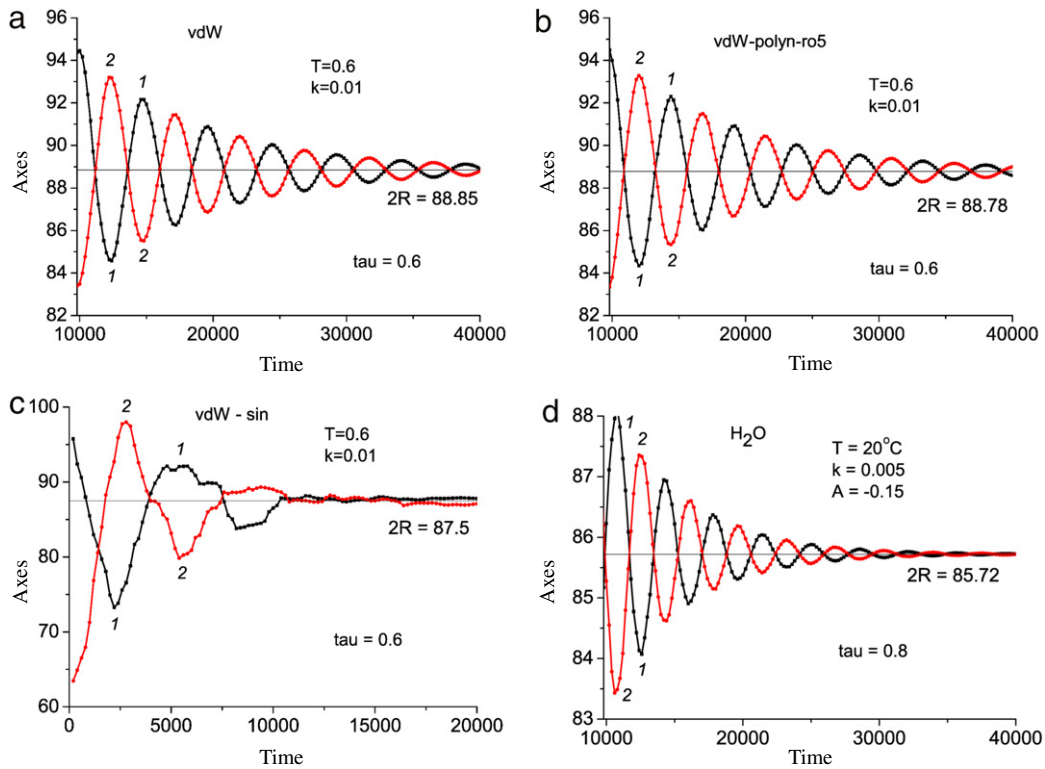


Fig. 8. Droplet oscillations in LBE simulations. (a) Van der Waals equation of state. $\tilde{T} = 0.6$. (b) Interpolation by Eq. (30) with the set (32). $\tilde{T} = 0.6$. (c) Interpolation by Eq. (18). $\tilde{T} = 0.6$. (d) Interpolation of the isotherm for EOS of water at 20 °C in the form (30) with the set (31). Curves 1 and 2 are the X and Y axes of the oscillating droplet, respectively.

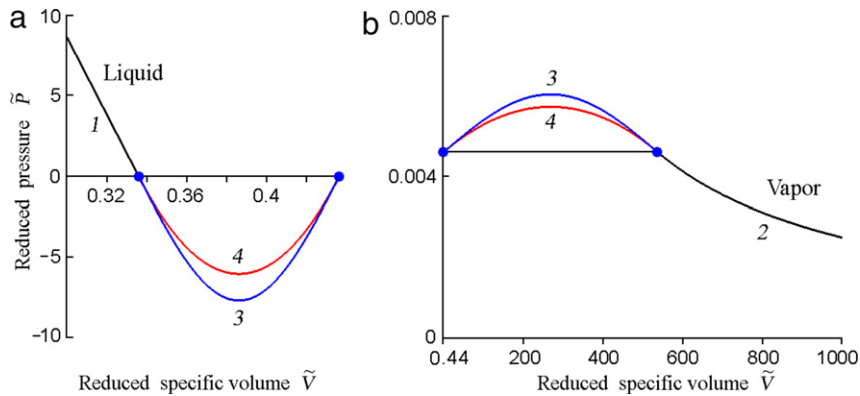


Fig. 9. Isotherm of water at the temperature 100 °C on the P - V diagram. Curves 1 and 2 are the liquid and vapor wings of the real isotherm [8]. Curves 3 and 4 are the piecewise interpolations of the isotherm in the sinusoidal form (18) and in polynomial form (25), respectively. The reduced saturation pressure $\tilde{P}_0 = 0.0046$.

The example of the reconstruction of isotherm at the relatively small temperature 20 °C, using the interpolation of the isotherm in the form (30) with the set of power exponents (31), is shown in Fig. 10. The real value of the liquid-to-vapor density ratio on the binodal curve is $\approx 58\,000$.

The coexistence of the vapor and liquid phases for a flat interface are studied in the LBE simulations at different temperatures for pure water with the real EOS [8]. To ensure the numerical stability of LBE simulations for water, we are forced to use the value $k = 0.005$, which is twofold less than for simulations with the van der Waals equation of state. The parameter $A = -0.15$ is used in these simulations. The results (particularly, the reduced specific volumes of the liquid and vapor phases and the reduced pressure on the binodal curve) obtained in the LBE simulations for the different interpolations are given in Table 5. Here, the values for real EOS of water are also shown. As pointed out earlier in [7], there is excellent agreement for the liquid branch of the binodal curve. It should be noted that the results obtained in the LBE simulations at the temperatures 100 and 300 °C agree well with the data on the vapor branch of the binodal curve for all interpolations.

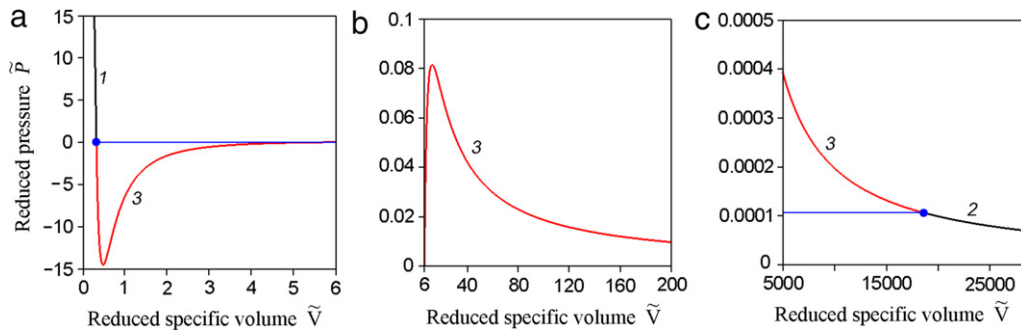


Fig. 10. Isotherm of H₂O at the temperature 20 °C. Curves 1 and 2 are the liquid and vapor wings of the real isotherm. Curve 3 is the interpolation of the isotherm in the form (30) with the set (31). The saturation pressure $\tilde{p}_0 = 0.000106$.

Table 5

Reduced specific volume and reduced pressure on the binodal curve for the real EOS of water.

$T, ^\circ\text{C}$	Lattice Boltzmann simulations			EOS
	Eq. (18)	Eq. (25)	Eq. (30), set (31)	
	Reduced specific volume of the liquid state			
20	0.32255	0.32255	0.32255	0.32255
50	0.32585	0.32585	0.32585	0.32585
100	0.33596	0.33596	0.33596	0.33596
300	0.45205	0.45209	0.45214	0.45209
	Reduced specific volume of the vapor state			
20	18 565	19 065	14 480	18 597
50	3779	3890	3410	3873
100	562.3	532.4	532.8	538.3
300	6.936	6.977	7.013	6.974
	Reduced pressure			
20	0.000106	0.000103	0.000136	0.000106
50	0.000573	0.000557	0.000635	0.000559
100	0.00440	0.00464	0.00463	0.00460
300	0.3906	0.3891	0.3878	0.3892
	Number of nodes in interface layer			
20	25	25	7	
50	25	25	7	
100	19	24	9	
300	21	23	18	

At lower temperatures, the interpolation in the form (30) with the set (31) gives somewhat smaller values of the specific volumes (up to 22% at 20 °C) and somewhat higher saturation pressure (up to 30% at 20 °C) than for real EOS of water.

The binodal curve for the real EOS of water and the results obtained in the LBE simulations for the interpolation (29) with the set (31) are shown in Fig. 11.

The method proposed in the present paper is used to simulate two-phase systems with the real EOS. For example, the liquid droplets in a saturated vapor (Fig. 12) are simulated for pure water at relatively small temperatures $T = 20\text{ }^\circ\text{C}$ ($\tilde{T} = 0.453$). Unfortunately, the nonsmooth interpolations cannot ensure an exact circular form of a stationary liquid droplet in a saturated vapor. In these cases, the shape of the droplet looks rather like a smoothed octagon (Fig. 12(a)). Obviously, the droplet has a round shape (Fig. 12(b)) for the smooth interpolation (29) with the set (31). This fact confirms the isotropy of the finite difference approximation (11) of the total force acting on a node. All smooth interpolations of the isotherm show similar macroscopic behavior of two-phase systems.

The LBE simulations of droplet oscillations are carried out for water at 20 °C using the interpolation of the isotherm by (30) with the set (31). The results are shown in Fig. 8(d). The deviation of the period of oscillations from the theoretical value is about 20% and is given in Table 4. The larger deviation, in comparison with the deviations for the vdW EOS, can be explained by the larger viscosity of the fluid. In the simulation for H₂O, the Reynolds number is twofold less than for fluid with the vdW EOS.

The results of the classical test for spinodal decomposition of a fluid and generation of two-phase vapor–liquid system for the real EOS of water. These isothermal simulations are carried out at the temperature 20 °C for different initial density of the fluid ρ_0 using the interpolation of the isotherm in the form (30) with the set (31). The results are shown in Figs. 13 and 14.

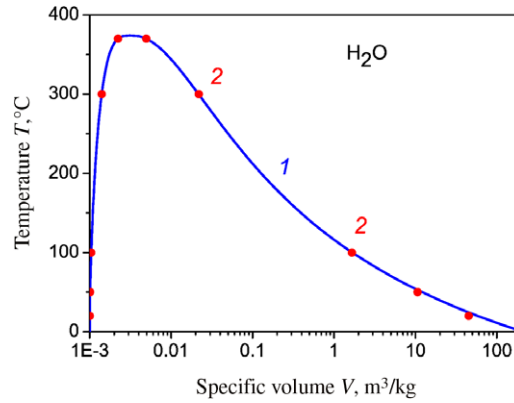


Fig. 11. Binodal curve for the real EOS of water. Curve 1 is the tabular data. Points 2 are the results of the LBE simulations for the flat stationary vapor–liquid interface. Interpolation of the isotherms by Eq. (30) with the set (31).

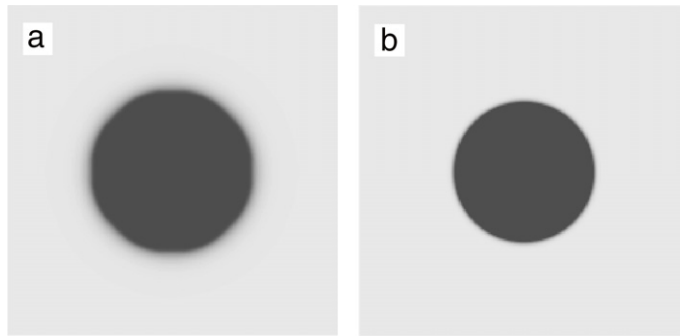


Fig. 12. Droplets of H₂O in saturated vapor at 20 °C. (a) Droplet for nonsmooth interpolation of the isotherm in the form (25). (b) Droplet of size $R = 44$ for smooth interpolation of the isotherm in the form (30) with the set (31). $k = 0.005$, $A = -0.15$, $\tau = 0.8$.

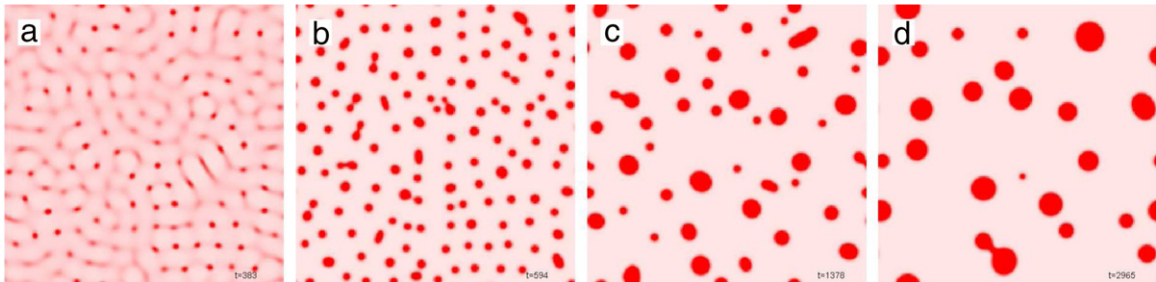


Fig. 13. Two-phase vapor–liquid system of H₂O at the late stages of the spinodal decomposition at 20 °C (liquid droplets are shown in dark color). The initial density of the fluid $\rho_0 = 0.3$. $k = 0.005$, $A = -0.15$, $\tau = 0.8$. $t = 400$ (a), 600 (b), 1400 (c), 3000 (d).

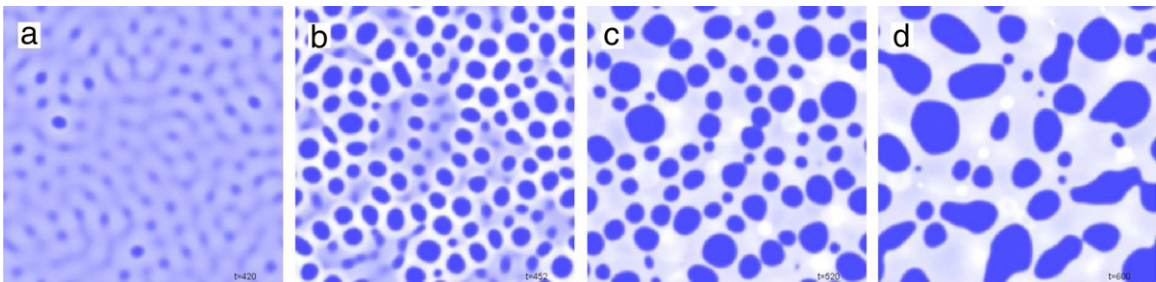


Fig. 14. Two-phase vapor–liquid system of H₂O at the late stages of the spinodal decomposition at 20 °C (vapor bubbles are shown in dark color). The initial density of the fluid $\rho_0 = 1.9$. $k = 0.005$, $A = -0.15$, $\tau = 0.8$. $t = 420$ (a), 450 (b), 520 (c), 600 (d).

6. Conclusions

The method of correct incorporation of the EOS for real fluids into the LBE model includes:

- The smooth extrapolation of the experimental data to the metastable regions of the fluid states and construction of the isotherm in the “prohibited” region, in accordance with the Maxwell rule.
- The isotropic finite difference approximation of the pseudo-potential gradient on a lattice.
- The method of exact difference for the implementation of the body force term.
- A relatively small $\Delta t/h$ ratio, required for the numerical stability of the LBE algorithm.

Several types of interpolations of the isotherms for real fluids in the region below the binodal curve are proposed. The sinusoidal interpolation (18) and the polynomial interpolation (25) can be found analytically. Unfortunately, these interpolations are nonsmooth at $V = V_0$ and cannot be used in nonstationary problems. The parameters of the interpolations by the spline functions (26) and (29), as well as for polynomial interpolations (30), can be found only numerically.

Our method allows one to obtain the values of the liquid and vapor densities at the interface corresponding to the saturated curve of real fluids with high accuracy. At low temperatures, the value of the liquid-to-vapor density ratio in the LBE simulations can be very high, in accordance with the EOS of real fluids.

The surface tension depends on the form of the interpolation of the isotherm under the binodal curve. Hence, the value of surface tension can be varied in some range by changing the interpolation curve.

Thus, we propose a way to construct the isotherm curve in the region where data cannot be obtained experimentally.

References

- [1] X. Shan, H. Chen, Lattice Boltzmann model for simulating flows with multiple phases and components, *Phys. Rev. E* 47 (3) (1993) 1815–1819.
- [2] M.R. Swift, W.R. Osborn, J.M. Yeomans, Lattice Boltzmann simulation of nonideal fluids, *Phys. Rev. Lett.* 75 (5) (1995) 830–833.
- [3] Y.H. Qian, S. Chen, Finite size effect in lattice-BGK models, *Internat. J. Modern Phys. C* 8 (4) (1997) 763–771.
- [4] R. Zhang, H. Chen, Lattice Boltzmann method for simulations of liquid–vapor thermal flows, *Phys. Rev. E* 67 (6) (2003) 066711.
- [5] A.L. Kupershtokh, Simulation of flows with liquid–vapor interfaces by the lattice Boltzmann method, *Vestnik NGU (Quart. J. Novosibirsk State Univ.), Ser.: Math. Mech. Inform.* 5 (3) (2005) 29–42 (in Russian).
- [6] A.L. Kupershtokh, D.I. Karpov, D.A. Medvedev, C.P. Stamatelatos, V.P. Charalambakos, E.C. Pyrgioti, D.P. Agoris, Stochastic models of partial discharge activity in solid and liquid dielectrics, *IET Sci. Meas. Technol.* 1 (6) (2007) 303–311.
- [7] A.L. Kupershtokh, D.A. Medvedev, D.I. Karpov, On equations of state in a lattice Boltzmann method, *Comput. Math. Appl.* 58 (5) (2009) 965–974.
- [8] The IAPWS industrial formulation 1997 for the thermodynamic properties of water and steam, Water/Steam Thermodynamic Surface on the WEB-site of Moscow Power Engineering Institute, Technical University. <http://twf.mpei.ac.ru/MCS/Worksheets/WSP/VTPs.xmcd>.
- [9] G.R. McNamara, G. Zanetti, Use of the Boltzmann equation to simulate lattice-gas automata, *Phys. Rev. Lett.* 61 (20) (1988) 2332–2335.
- [10] F.J. Higuera, J. Jiménez, Boltzmann approach to lattice gas simulations, *Europhys. Lett.* 9 (7) (1989) 663–668.
- [11] Y.H. Qian, D. d’Humières, P. Lallemand, Lattice BGK models for Navier–Stokes equation, *Europhys. Lett.* 17 (6) (1992) 479–484.
- [12] D. d’Humières, Generalized lattice-Boltzmann equations, in: B.D. Shizgal, D.P. Weaver (Eds.), *Rarefied Gas Dynamics: Theory and Simulations*, in: *Progress in Astronaut and Aeronaut*, vol. 159, AIAA, Washington, DC, 1992, pp. 450–458.
- [13] P. Lallemand, Li-Shi Luo, Theory of the lattice Boltzmann method: dispersion, dissipation, isotropy, Galilean invariance, and stability, *Phys. Rev. E* 61 (6) (2000) 6546–6562.
- [14] A.L. Kupershtokh, Calculations of the action of electric forces in the lattice Boltzmann equation method using the difference of equilibrium distribution functions, in: *Proc. 7th Int. Conf. on Modern Problems of Electrophysics and Electrohydrodynamics of Liquids*, St. Petersburg State University, St. Petersburg, Russia, 2003, pp. 152–155.
- [15] A.L. Kupershtokh, New method of incorporating a body force term into the lattice Boltzmann equation, in: *Proc. 5th International EHD Workshop*, University of Poitiers, Poitiers, France, 2004, pp. 241–246.
- [16] A.L. Kupershtokh, Incorporating a body force term into the lattice Boltzmann equation, *Vestnik NGU (Quart. J. Novosibirsk State Univ.), Ser.: Math. Mech. Inform.* 4 (2) (2004) 75–96 (in Russian).
- [17] A.L. Kupershtokh, Criterion of numerical instability of liquid state in LBE simulations, *Comput. Math. Appl.* 59 (7) (2010) 2236–2245.
- [18] J.C. Slater, *Introduction to Chemical Physics*, McGraw-Hill Book Company, New York, 1939.
- [19] L.D. Landau, E.M. Lifshitz, *Fluid Mechanics*, Pergamon Press, Oxford, 1959.